

Article

A Model Development for Thermal and Solutal Transport Analysis of Non-Newtonian Nanofluid Flow over a Riga Surface Driven by a Waste Discharge Concentration

Javali Kotresh Madhukesh ¹, Vinutha Kalleshchar ², Chandan Kumar ¹, Umair Khan ^{3,4,*}, Kallur Venkat Nagaraja ¹, Ioannis E. Sarris ⁵, El-Sayed M. Sherif ⁶, Ahmed M. Hassan ⁷ and Jasgurpreet Singh Chohan ⁸

¹ Department of Mathematics, Amrita School of Engineering, Amrita Vishwa Vidyapeetham, Bengaluru 560035, India; madhukeshjk@gmail.com (J.K.M.); chandanrko786@gmail.com (C.K.); kv_nagaraja@blr.amrita.edu (K.V.N.)

² Department of Studies in Mathematics, Davangere University, Davangere 577002, India; vinuthavinu392@gmail.com

³ Department of Computer Science and Mathematics, Lebanese American University, Byblos 1401, Lebanon

⁴ Department of Mathematics and Social Sciences, Sukkur IBA University, Sukkur 65200, Sindh, Pakistan

⁵ Department of Mechanical Engineering, University of West Attica, 12244 Athens, Greece; sarris@uniwa.gr

⁶ Mechanical Engineering Department, College of Engineering, King Saud University, P.O. Box 800, Al-Riyadh 11421, Saudi Arabia; esherif@ksu.edu.sa

⁷ Mechanical Engineering, Future University in Egypt, New Cairo 11835, Egypt; ahmed.hassan.res@fue.edu.eg

⁸ Department of Mechanical Engineering and University Centre for Research & Development, Chandigarh University, Mohali 140413, India; jasgurpreet.me@cumail.in

* Correspondence: umairkhan@iba-suk.edu.pk



Citation: Madhukesh, J.K.; Kalleshchar, V.; Kumar, C.; Khan, U.; Nagaraja, K.V.; Sarris, I.E.; Sherif, E.-S.M.; Hassan, A.M.; Chohan, J.S. A Model Development for Thermal and Solutal Transport Analysis of Non-Newtonian Nanofluid Flow over a Riga Surface Driven by a Waste Discharge Concentration. *Water* **2023**, *15*, 2879. <https://doi.org/10.3390/w15162879>

Academic Editor: Hirakendu Basu

Received: 30 June 2023

Revised: 25 July 2023

Accepted: 26 July 2023

Published: 9 August 2023



Copyright: © 2023 by the authors. Licensee MDPI, Basel, Switzerland. This article is an open access article distributed under the terms and conditions of the Creative Commons Attribution (CC BY) license (<https://creativecommons.org/licenses/by/4.0/>).

Abstract: Wastewater discharge plays a vital role in environmental management and various industries. Water pollution control and tracking are critical for conserving water resources and maintaining adherence to environmental standards. Therefore, the present analysis examines the impact of pollutant discharge concentration considering the non-Newtonian nanofluids over a permeable Riga surface with thermal radiation. The analysis is made using two distinct kinds of non-Newtonian nanofluids: second-grade and Walter's liquid B. The governing equations are made using the applications of boundary layer techniques. Utilizing the suitable similarity variable reduces the formulated governing equations into an ordinary differential set of equations. The solutions will be obtained using an efficient numerical technique and the significance of various dimensionless constraints on their individual profiles will be presented using graphical illustrations. A comparative analysis is reported for second-grade and Walter's liquid B fluids. The results show that the porous factor declines the velocity profile for both fluids. Radiation and external pollutant source variation constraints will improve thermal and concentration profiles. The rate of thermal distribution improved with the rise in radiation and solid volume factors. Further, essential engineering factors are analyzed. The outcomes of the present study will help in making decisions and putting efficient plans in place to reduce pollution and safeguard the environment.

Keywords: Riga surface; second grade fluid; Walter B fluid; nanofluid; thermal radiation; pollutant concentration

1. Introduction

The Riga plate is a flat surface made of electrical and permanent magnetization. The Riga surface is an external factor used to minimize drag and control fluid flow. Because of the magnetoelectric fields this device generates, Lorentz forces allow fluid flow control. Flexible electronics, monitoring for earthquake disasters, reducing drag on ships, robots, smart energy networks, electromechanical devices, recuperating energy, thermal nuclear

reactors, heat exchange systems, solar-powered equipment, and generators for electricity are some of the applications of Riga plates. Many academics have carried out studies on fluid flows in the area of the Riga surface. Asogwa et al. [1] scrutinized the character of Dufour, thermal production, and activation energy on the movement of the hyperbolic tangent nano-based liquid via the Riga body surface. Madhukesh et al. [2] scrutinized the consequence of thermophoretic particle decomposition of a Casson hybrid nanoliquid subjected to laminar, uniform flow generated by a Riga surface in the attendance of a porous media. Xu et al. [3] explored the consequence of the magnetic field, mixed convection, and thermal sink/source on a fourth-grade liquid circulation around a Riga body. Asogwa et al. [4] excavated the observed outcome of the heat sink and chemical reaction through a Riga surface of Casson nanofluids. Alshehri et al. [5] deliberated the thermal distribution rate, including the Cattaneo–Christov heat flux model, with the effect of fluid viscosity, magnetic field, and porous medium of hybrid nanofluids through a Riga surface. Prasad et al. [6] examined the impact of Brownian motion, viscosity, velocity slip, and first-order chemical reaction of thermal and mass distribution of nanoliquids through a Riga plate. Mandal and Pal [7] conducted a study on nanofluids having a mixture of convective and quadratic radiative movements over a decreasing Riga surface with convective boundary conditions and slip velocities

The term “Second-grade fluid” refers to a subtype of non-Newtonian fluid. And, the velocity sector displays up to two derivatives in the strain-and-stress tensor relationship. In contrast to Newtonian fluids, the equations controlling flow generally are significantly nonlinear. Non-Newtonian fluids have an inclusive array of industrial applications, together with plastic film illustration, fabricating fiberglass, creating paper, manufacturing plastic sheets, and several others. These factors make investigating non-Newtonian fluids a fascinating field for mathematical researchers, computer science researchers, and technologists. The convection of second-grade fluid in the appearance of a magnetic field along a flat plate using Prabhakar fractional derivative was studied by Ali et al. [8]. Gowda et al. [9] examined the second-grade fluid along with significant impact of chemical reactions and activation energy over the Marangoni layer boundary conditions. Utilizing the Gear-generalized differential quadrature assessment of oscillating convective Taylor–Couette movement, second-grade fluid impacted by Lorentz and Darcy–Forchheimer quadratic drag forces was examined by Xia et al. [10]. The exact solution of the unsteady second-grade fluid model related to oscillating shear stress on the sphere is surveyed by Fetecau et al. [11]. Shah et al. [12] studied the impression of thermophoresis particle deposition of a second-grade fluid with the variation of viscosity, concentration diffusivity, and thermal conductivity with convective boundary conditions. Khan et al. [13] examined the impact of second-grade nanoliquid moving into two infinite plates while it reacts chemically. Over a nonlinear extending sheet, Hayat [14] investigated the magnetohydrodynamic motion of a second-grade nanofluid.

One of the momentous non-Newtonian liquid subsidiaries is Walter’s liquid B fluid. The formative equations in non-Newtonian liquids are more intricate. Hence, it is crucial to build more complicated equations. When dealing with the highly nonlinear Walter’s liquid B fluid model, it is quite complicated. One of the better models for describing the properties of a viscoelastic fluid is the Walter’s liquid B fluid model, which has a brief memory coefficient and limits viscosity at low shear rates. Elasticity features are helpful in comprehending non-Newtonian performance, and fundamental equations can frequently provide significant support in figuring out rheological qualities. Science has shown that this model is proficient in replicating the attributes of viscoelastic polymers, hydrocarbon molecules, paints, and other fluids in disparate fields. Non-Newtonian fluids are becoming increasingly significant in biology, petroleum-based substances, fluid dynamics, chemical fields, and material science. With the assistance of viscoelastic flow substances, noise reduction, mitigation of shock, and vibration isolation are performed. Walter’s liquid B fluid model through a sheet in the occurrence of porous medium with the impact of the Soret and Dufour local thermal nonequilibrium is studied by Kumar et al. [15]. Lorentz

force, thermomigration, and random motion of small particles in radiative reactive Walter's liquid B fluid brought on by mixed convection gyrotactic microorganisms are inspected by Wakif et al. [16]. Thermal stratifications have been utilized by Siddique et al. [17] to study the thermography of ferromagnetic Walter's liquid B fluid. Qaiser et al. [18] scrutinized Walter's liquid B fluid through an extending sheet with mass suction and magnetic field with Newtonian heating. Chu et al. [19] deliberated the interaction between Walter B nanoliquid movement across an extending sheet and TPD (thermophoresis particle deposition) with the influence of the pressure and buoyancy forces when there is a magnetic field.

Nanofluid is a base fluid combined with unique nanoparticles. In nanofluids, nanoparticles are formed of carbides, oxides, metals, etc. Water, oil, ethylene glycol, and other fundamental liquids are frequently considered base liquids. The term Nanofluid was first developed by Choi [20] in 1995. The basic liquid's capacity to transmit heat is improved when nanoparticles are added. It has several practical uses in numerous sectors, especially the medicine, engineering, and chemical sciences. And, nanofluids have applications in industries, including biomedical, automotive, transportation, electrical, the distribution of drugs, real-time chemical monitoring of brain function, technology, and the removal of tumors. Researchers have also been more attentive to nanofluid applications of nanoliquids. Khan et al. [21] scrutinized the importance of Lorentz forces in a hybrid nanofluid movement caused by a stretched sheet contaminant. Gkoutas et al. [22] examined how a nanofluid affected printed-circuit thermal transfer. Madhukesh et al. [23] deliberated the result of heat production and absorption on a nanoliquid flowing through a stretching surface in the incidence of activation energy. Haq et al. [24] examined the effect of heat sink/source, porous medium, and homogeneous and heterogeneous interaction on hybrid nanofluids of various geometries. Dogonchi et al. [25] studied the characteristics of nanofluids inside the irregular triangular enclosure in the appearance of a magnetism.

A phenomenon in which the transfer of thermal energy occurs is known as thermal radiation, and it disperses thermal energy through fluid particles. By accelerating thermal diffusivity, thermal radiation increases the temperature. Thermal radiation is frequently used in modern heat exchange systems that transport heat at exceedingly high temperatures. Thermal radiation also considerably impacts controlling the heat transfer mechanism in the polymer manufacturing industries. Fluid flow with thermal radiation is significant for applications in engineering fields, such as managing thermal distribution in the nuclear reactor and handling the thermal distribution in the polymer. The impression of thermal radiation on the space industry and high-temperature operations is well established. Gireesha et al. [26] investigated the three-dimensional Maxwell nanofluid motion with convective boundary conditions in addition to the occurrence of a magnetic field. Ramesh et al. [27] examined the movement of hybrid carbon nanotubes on a stagnation point around a spinning sphere when heat radiation and thermophoretic particle deposition were present. Taking magnetic force effects into account, Atashafrooz et al. [28] simulated the convective and radiative thermal transfer of a hybrid nanofluid flowing inside a trapezoidal container. Oke et al. [29] examined the effects of a magnetic field and thermal radiation on 3D hybrid nanofluid movement within the boundary layer. Alzahrani et al. [30] scrutinized the impact of thermal radiation on the transmission of heat in a Casson nanoliquid movement in a plane wall that exhibits suction under a slip boundary condition. Prasannakumara and Shashikumar [31] used numerical analysis to examine the boundary layer movement and transfer of heat of a tiny fluid material across a nonlinear stretched sheet in the existence of thermal radiation. Thumma et al. [32] examined the impact of Coriolis force on the movement of a nanoliquid in thermal radiation and heat generation/absorption. Hydrothermal behaviors of nanofluid flow in a trapezoid recess were analyzed using the second law of principles by Atashafrooz et al. [33].

Pollutant concentration describes the contaminants in water, air, or soil volume. Pollutants have a more significant impact on the health of people, animals, and living things. The transport of contaminants is challenging to forecast precisely. Certain research studies have produced initial conclusions on how external pollutant source characteristics affect

the concentration of pollutants. Makinde et al. [34] studied pollutant transportation in rivers using partial differential equations. Cintolasi et al. [35] scrutinized the complicated connection between heat and inertial factors within the canyon, especially the effects on turbulence characteristics and pollution remediation techniques. Chinyoka and Makinde [36] examined the nonlinear spreading of a pollutant released by an external source through the laminar liquid circulation of an incompressible liquid in a channel. Southerland et al. [37] investigated the health risks of air pollution in towns. Chinyoka and Makinde [38] examined the dispersion of a polymeric impurity emanating from an external source into the laminar motion of a Newtonian solution moving via a rectangular channel.

Relative to the above-served literature, work has yet to be carried out to examine the impact of pollutant discharge concentration considering the non-Newtonian nanoliquids over a permeable Riga surface with thermal radiation. The governing expressions are made by taking the considerable impacts, and resultant equations are solved numerically using an efficient numerical scheme. The numerical outcomes are shown with the help of graphs, and the results are discussed in detail. The outcomes of this study will contribute to an enhanced understanding of waste management, temperature transportation, and distribution optimization, which increase the quality of decision-making and planning for environmental protection and environmentally friendly engineering.

The present investigation is carried out to find the answers to the following research insight questions:

1. How does the modified Hartmann number impact the velocity profile in the presence of second-grade fluid and Walter’s liquid B fluid?
2. What are the behavioral changes observed in the concentration profile when external pollutant source variation parameter are varied?
3. How will the local pollutant external source parameter and solid volume fractions influence the mass transfer rate?

2. Mathematical Formulation

Consider a steady, two-dimensional, laminar flow of non-Newtonian second-grade fluid and Walter’s liquid B fluid circulating across a Riga surface. The Riga surface moves with a free stream velocity $\bar{u} = U_w = xa$, in x -direction ($a > 0$) (see Figure 1). T_w , T_∞ , C_w and C_∞ terms represent the surface and ambient temperature of the Riga surface and surface and ambient concentration, respectively. The Riga plate is considered under the presence of electromagnetic force $F_m^* = (F_m^*, 0, 0) : [F_m^* = \exp(-\frac{\pi}{c}y) \frac{\pi j_0 M_0}{8\rho_{nf}}]$. Further, thermal radiation and external pollutant concentrations are considered in the temperature and concentration equation.

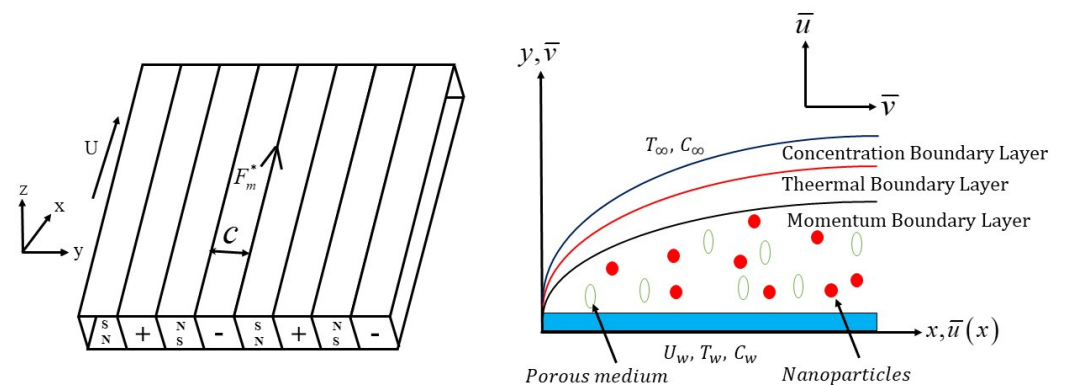


Figure 1. Geometry of the flow.

Taking the above-stated assumptions, the governing equations are as follows (see [7,14,19,36,38]):

$$\frac{\partial \bar{u}}{\partial x} + \frac{\partial \bar{v}}{\partial y} = 0, \tag{1}$$

$$\begin{aligned} \bar{u} \frac{\partial \bar{u}}{\partial x} = & \frac{\mu_{nf}}{\rho_{nf}} \frac{\partial^2 \bar{u}}{\partial y^2} + \frac{\pi j_0 M_0}{8 \rho_{nf}} \exp\left(-\frac{\pi}{c} y\right) - \frac{\nu_{nf}}{K^*} \bar{u} - \bar{v} \frac{\partial \bar{u}}{\partial y} \\ & \pm \frac{\alpha_1^*}{\rho_{nf}} \left(\frac{\partial^3 \bar{u}}{\partial x \partial y^2} - \frac{\partial^3 \bar{u}}{\partial y^2 \partial x} + \bar{u} \frac{\partial^3 \bar{u}}{\partial x \partial y^2} + \bar{v} \frac{\partial^3 \bar{u}}{\partial y^3} \right), \end{aligned} \tag{2}$$

$$\bar{u} \frac{\partial T^*}{\partial x} + \bar{v} \frac{\partial T^*}{\partial y} = \alpha_{nf} \frac{\partial^2 T^*}{\partial y^2} - \frac{1}{(\rho C_p)_{nf}} \frac{\partial q_r}{\partial y}, \tag{3}$$

$$\bar{u} \frac{\partial C}{\partial x} - D_f \frac{\partial^2 C}{\partial y^2} = Q^* \exp(b_3^*(C - C_\infty)) - \bar{v} \frac{\partial C}{\partial y}, \tag{4}$$

with the BCs

$$\left. \begin{aligned} y = 0 : \bar{u} = U_w, \bar{v} = 0, T^* = T_w, C = C_w \\ y \rightarrow \infty : \bar{u} \rightarrow 0, \frac{\partial \bar{u}}{\partial y} \rightarrow 0, T^* \rightarrow T_\infty, C \rightarrow C_\infty \end{aligned} \right\}. \tag{5}$$

The following set of similarity transformations are introduced:

$$\psi = x \sqrt{av_f} f, \bar{u} = x f' a, \bar{v} = -\sqrt{av_f} f, \eta = \sqrt{\frac{1}{a^{-1} \nu_f}} y, \theta = \frac{T^* - T_\infty}{T_w - T_\infty}, \chi = \frac{C - C_\infty}{C_w - C_\infty}. \tag{6}$$

From the overhead equations, the terms α_1^* denotes the material constant. $\alpha_1^* > 0$ and $\alpha_1^* < 0$ correspondingly denote second-grade fluid and Walter’s liquid B fluid, respectively. x and y are the directions. \bar{u} and \bar{v} are the velocity components. ν is the kinematic viscosity, ρ is the density, and j_0 and M_0 are the applied current density in electrodes and magnetization of permanent magnets, K^* is the permeability of the porous medium, c is the width of the electrodes, T^* is the temperature, α is the thermal diffusivity, C_p is the heat capacitance, k is the thermal conductivity, D_f is the diffusivity, and C is the concentration. q_r is the radiation heat flux. Q^* and b_3^* denote pollutant external source variation parameters.

From Equation (3), the radiation heat flux term is defined (using Rosseland approximation (see [39])) as $q_r = -\frac{4\sigma^*}{3k^*} \left(\frac{\partial T^{*4}}{\partial y} \right)$.

The term T^{*4} is a linear function of temperature. Expanding the term T^{*4} up to infinity, we get

$$T^{*4} = T_\infty^4 + 4(T^* - T_\infty)T_\infty^3 + 6(T^* - T_\infty)^2 T_\infty^2 + \dots$$

Excluding the higher order components except $(T^* - T_\infty)$ in the above equation, we get $T^{*4} = 4T_\infty^3 T^* - 3T_\infty^4$; then, the expression q_r takes the form

$$q_r = -\frac{16\sigma^* T_\infty^3}{3k^*} \left(\frac{\partial T^*}{\partial y} \right).$$

By substituting the above term, Equation (3) takes the following form

$$\bar{u} \frac{\partial T^*}{\partial x} + \bar{v} \frac{\partial T^*}{\partial y} = \left(\frac{k_{nf}}{(\rho C_p)_{nf}} + \frac{16\sigma^* T_\infty^3}{3k^*} \right) \frac{\partial^2 T^*}{\partial y^2}. \tag{7}$$

By using Equation (6), Equations (1), (2), (4), (5) and (7) take the form

$$\frac{f'''}{A_1^* A_2^*} \pm \frac{K_1^*}{A_2^*} [2f' f''' - f f'''' - (f'')^2] + \frac{Q_1^*}{A_2^*} \exp(-\eta \beta_1^*) - \frac{\lambda_1^*}{A_1^* A_2^*} f' + f f'' - (f')^2 = 0, \tag{8}$$

$$\left[\frac{k_{nf}}{k_f} + \frac{4}{3} Rd_1^* \right] \frac{\theta''}{Pr A_3^*} + f \theta' = 0, \tag{9}$$

$$\frac{\chi''}{Sc_1^*} + f\chi' + \delta_1^* \exp(\gamma_1^* \chi) = 0, \tag{10}$$

with BCs

$$\left. \begin{aligned} f(\eta)_{\eta=0} = 0, f'(\eta)_{\eta=0} = 1, \theta(\eta)_{\eta=0} = 1, \chi(\eta)_{\eta=0} = 1 \\ f'(\eta)_{\eta=\infty}, f''(\eta)_{\eta=\infty} = 0, \theta(\eta)_{\eta=\infty} = 0, \chi(\eta)_{\eta=\infty} = 0 \end{aligned} \right\} \tag{11}$$

From the above Equations (8)–(10), the dimensionless constraints are listed in Table 1.

Table 1. List of dimensionless constraints.

Sl. No	Parameter Definition	Parameter Name
01	$K_1^* = \frac{\alpha_1^* a}{\rho_f \nu_f}$	Viscoelastic constraint $K_1^* > 0$ second-grade fluid $K_1^* < 0$ Walter’s liquid B fluid
02	$Q_1^* = \frac{\pi j_0 M_0}{8 \rho_f a U_w}$	Modified Hartmann number
03	$\beta_1^* = \sqrt{\frac{\pi^2 \nu_f}{c^2 a}}$	Parameter related to width and magnitude of electrodes
04	$\lambda_1^* = \frac{\nu_f}{K^* a}$	Porous constraint
05	$Rd_1^* = \frac{4\sigma^* T_\infty^3}{k^* k_f}$	Radiation constraint
06	$Pr = \frac{\nu_f}{\alpha_f}$	Prandtl number
07	$\delta_1^* = \frac{Q}{a(C_w - C_\infty)}$	Parameter related to local pollutant external source
08	$\gamma_1^* = b_3(C_w - C_\infty)$	Parameter related to external pollutant source variation
09	$Sc_1^* = \left(\frac{\nu_f}{D_f}\right)$	Schmidt number
10	$Re = \frac{x^2 a}{\nu_f}$	Local Reynolds number
11		$A_1^* = (1 - \phi^*)^{2.5}$
12		$A_2^* = \left(1 - \phi^* + \phi^* \frac{\rho_s}{\rho_f}\right)$
13		$A_3^* = \left(1 - \phi^* + \phi^* \frac{(\rho C_p)_s}{(\rho C_p)_f}\right)$

The important engineering factor and its reduced form is provided as follows:

$$Cf = \frac{1}{\rho_f U_w^2} \left(\mu_{nf} \frac{\partial \bar{u}}{\partial y} \pm \alpha_1^* \left(\frac{\partial^2 \bar{u}}{\partial x \partial y} 2 + \bar{v} \frac{\partial^2 \bar{u}}{\partial y^2} + \frac{\partial^2 \bar{u}}{\partial x \partial y} \bar{u} \right) \right)_{y=0}, \tag{12}$$

$$Nu = - \frac{x \left(k_{nf} + \frac{16\sigma^* T_\infty^3}{3k^*} \right) \left(\frac{\partial T^*}{\partial y} \right)_{y=0}}{k_f (T_w - T_\infty)}, \tag{13}$$

$$Sh = - \frac{x D_f \left(\frac{\partial C}{\partial y} \right)_{y=0}}{D_f (C_w - C_\infty)}. \tag{14}$$

Using the Equation (6) in (12)–(14) the following equations are attained:

$$Cf = - \frac{1}{\sqrt{Re}} \left(f'''(0) f(0) K_1^* - \left(\frac{1}{A_1} \pm 3K_1^* f'(0) \right) f''(0) \right), \tag{15}$$

$$Nu = - \left(\frac{k_{nf}}{k_f} + \frac{4}{3} Rd_1^* \right) \theta'(0) \sqrt{Re}, \tag{16}$$

$$\frac{Sh}{\sqrt{Re}} = -\chi'(0). \tag{17}$$

3. Numerical Scheme

The transformed set of ODEs (8) to (10) and reduced boundaries, as stated in Equation (11), is challenging to obtain the analytical solution due to its high nonlinearity and two-point

boundary nature. So, the solution of these equations is traced using the efficient numerical method. For this, we can convert the set of higher-order equations into first-order:

$$\{f, f', f'', f'''\} = \{\omega_1, \omega_2, \omega_3, \omega_4\}$$

$$f''' = \frac{A_2^*}{K_1^* \omega_1} \left(\frac{\omega_4}{A_1^* A_2^*} \pm \frac{K_1^*}{A_2^*} [2\omega_2 \omega_4 - (\omega_3)^2] + \frac{Q_1^*}{A_2^*} \exp(-\eta \beta_1^*) - \frac{\lambda_1^*}{A_1^* A_2^*} \omega_2 \right) + \omega_1 \omega_3 - (\omega_2)^2 \tag{18}$$

$$\{\theta, \theta'\} = \{\omega_5, \omega_6\}$$

$$\theta'' = -Pr A_3^* \frac{\omega_1 \omega_6}{\left[\frac{k_{nf}}{k_f} + \frac{4}{3} Rd_1^* \right]} \tag{19}$$

$$\{\chi, \chi'\} = \{\omega_7, \omega_8\}$$

$$\chi'' = -(\omega_1 \omega_8 + \delta_1^* \exp(\gamma_1^* \omega_7)) Sc_1^* \tag{20}$$

and the BCs becomes

$$\begin{aligned} \omega_1(0) &= 0, \omega_2(0) = 1, \omega_3(0) = \varepsilon_1, \\ \omega_4(0) &= \varepsilon_2, \omega_5(0) = 1, \omega_6(0) = \varepsilon_3, \\ \omega_7(0) &= 1, \omega_8(0) = \varepsilon_4. \end{aligned} \tag{21}$$

The above equations are obtained using RKF-45 (Runge Kutta Fehlberg’s 4th–5th order), and the missing boundary values in Equation (20) are obtained via the shooting procedure. The values of the parameters are set to $Q_1^* = 0.01$, $\beta_1^* = 0.1$, $\lambda_1^* = 0.1$, $Rd_1^* = 0.1$, $\gamma_1^* = \delta_1^* = 0.01$, and $Sc_1^* = 0.8$; using the thermophysical characteristics and properties stated in Tables 2 and 3, the numerical solutions are obtained using 0.01 as a step size and 10^{-6} set for tolerance of error. Further, our present numerical scheme is validated by the works of [40–42] for some limiting parameters and obtained good agreement (see Table 4).

Table 2. List of thermophysical characteristics of nanofluids.

Thermophysical Characteristics	Name
$(\rho C_p)_{nf} = \left((1 - \phi^*) + \phi^* \frac{(\rho C_p)_s}{(\rho C_p)_f} \right) (\rho C_p)_f$	Specific heat capacity
$\mu_{nf} = \frac{\mu_f}{(1 - \phi^*)^{2.5}}$	Dynamic viscosity
$k_{nf} = \frac{(k_s + 2\phi^* k_s + 2k_f(1 - \phi^*))k_f}{k_s - \phi^* k_s + k_f(2 + \phi^*)}$	Thermal conductivity
$\rho_{nf} = \left(1 - \phi^* + \phi^* \frac{\rho_s}{\rho_f} \right) \rho_f$	Density

Table 3. List of thermophysical properties of nanofluids (see [43,44]).

Properties	Pr	C_p (Jkg ⁻¹ K ⁻¹)	k (kgms ⁻³ K ⁻¹)	ρ (kgm ⁻³)
SA(C ₆ H ₉ NaO ₇)	6.45	4175	0.6376	989
TiO ₂	-	686.2	8.9528	4250

Table 4. Assessment of numerical values $-\theta'(\eta)_{\eta=0}$ for variation in Pr with the absence of λ_1^* , K_1^* , Rd_1^* , ϕ^* , and Q_1^* .

Pr	Ishak et al. [42]	Abolbashari et al. [43]	Das et al. [44]	Present Numerical Outcome
0.72	0.8086	0.80863135	0.80876122	0.80876153
1.0	1.0000	1.00000000	1.00000000	1.00000000
3.0	1.9237	1.92368259	1.92357431	1.92357446
7.0	3.0723	3.07225021	3.07314679	3.07314636
10	3.7207	3.72067390	3.72067390	3.72067335

The numerical flowchart of the present numerical scheme is presented in Figure 2.

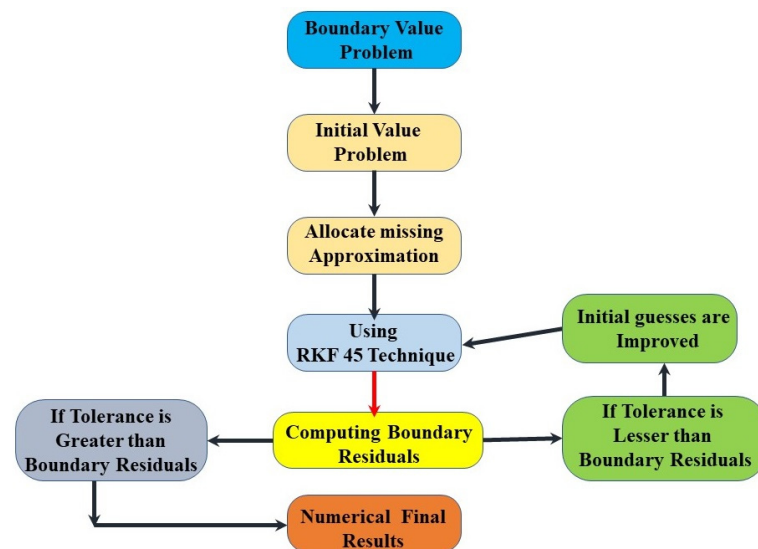


Figure 2. Structural flow of numerical scheme.

4. Results and Discussion

The present section explains the influence of various dimensionless constraints on their profiles. The analysis is made using the comparison of two different kinds of non-Newtonian nanoliquids in the presence of various factors. Further, the important engineering factors are analyzed and deliberated in detail.

Figure 3 illustrates the impact of the K_1^* (viscoelastic constraint) over f' (velocity) profile. The K_1^* plays a significant role in identifying the behavior of the liquids, especially in second-grade fluid and Walter’s liquid B fluid. The positive values of K_1^* will denote the second-grade fluid. The improvement in positive K_1^* values will significantly improve the f' profile. Second-grade fluid displayed shear-thinning behavior, which means the viscosity falls as the shear rate improves. As a result, increasing K_1^* improves the liquid’s capacity to move more freely, leading to greater velocities. The negative values of K_1^* signify the Walter’s liquid B fluid. The improvement in negative values K_1^* will decline the velocity. Walter’s liquid B fluid has a more complicated behavior, with larger negative values of K_1^* resulting in a greater viscosity and, thus, decreased velocity.

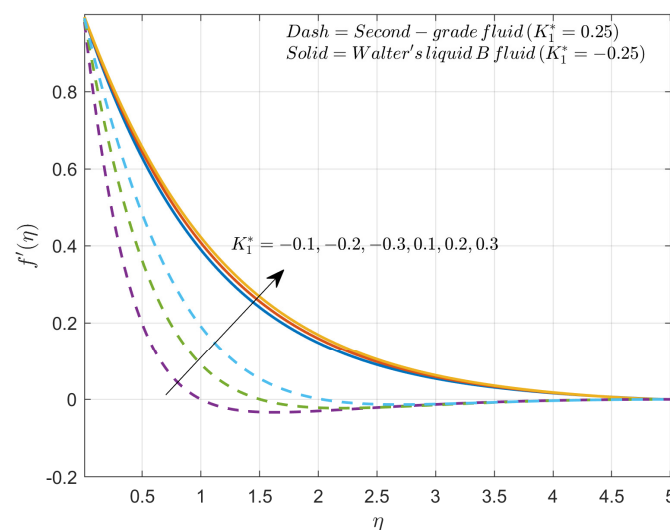


Figure 3. Influence of K_1^* on f' profile.

Figure 4 shows the variation in the velocity profile for improved values of the porous factor for both second-grade fluid and Walter’s liquid B fluid cases. The improved values

of porous factor will reduce the fluid velocity in both the cases. The rise in porous factor will exhibit the resistance caused by the porous surface which acts as a barrier to the flow of liquid. Further, the porous medium will promote the interaction between the liquid and surface of the object which improves the thickness of the boundary layer. It is observed that velocity is more in second-grade fluid than Walter’s liquid B fluid in the presence of the porous factor.

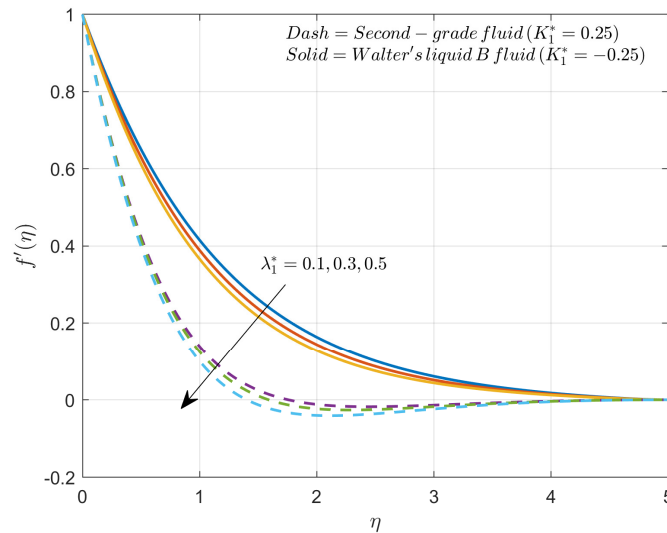


Figure 4. Influence of λ_1^* on f' profile.

Figure 5 illustrates the impact of the modified Hartmann number Q_1^* over the f' profile for second-grade fluid and Walter’s liquid B fluid scenarios. The improvement in Q_1^* will improve the velocity profile in the second-grade fluid case while the reverse behavior is seen in the case of Walter’s liquid B fluid. In case the of second-grade fluid, improved Q_1^* will improve the external electrical impact over the liquid which improves the ability of the circulation, while in Walter’s liquid B fluid an improved Q_1^* will improve the viscosity of the liquid due to an improved electrical field, making it more resistant to movement. In the presence of Q_1^* the two liquid models behave differently over the velocity profile.

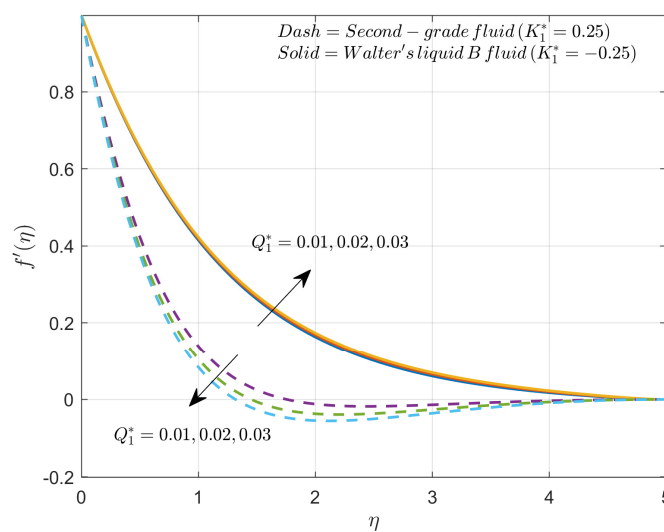


Figure 5. Influence of Q_1^* on f' profile.

The variation in the thermal θ profile for changing values of the radiation Rd_1^* parameter is illustrated in Figure 6. The improved values of Rd_1^* will exhibit enhancement in thermal distribution. The adoption of radiation constraints reduces the k^* , which improves

the radiative thermal flux coefficients and radiative heat transmission rates into the liquid. Because of the increased radiative thermal transmission, the extent of the thermal boundary layer is noticeable. For the given radiation, Rosseland’s diffusion manner raises the temperature of the fluid. It is observed that Walter’s liquid B fluid shows greater thermal distribution than second-grade fluid. The Walter’s liquid B fluid will exhibit higher thermal conductivity as well as thermal diffusivity when compared to second-grade fluid. These properties of Walter’s liquid B fluid result in more distribution of heat in the fluid system within the presence of Rd_1^* .

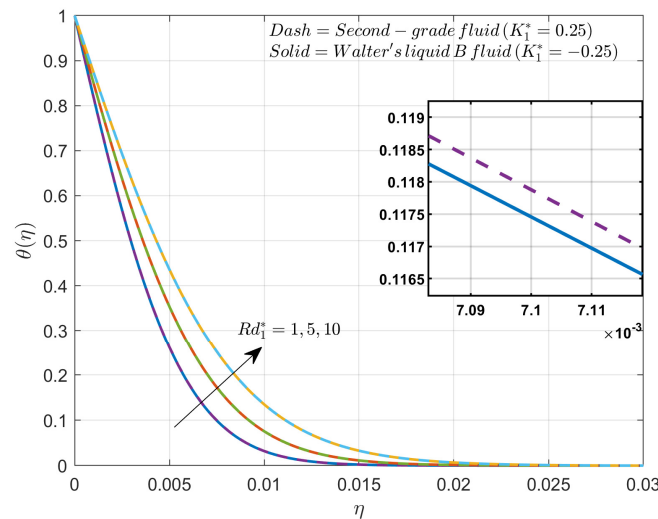


Figure 6. Influence of Rd_1^* on θ profile.

The impact of external pollutant source variation factor γ_1^* over the concentration χ profile is drawn in the Figure 7. The rise in γ_1^* will enhance the concentration in both second-grade fluid and Walter’s liquid B fluid cases. As γ_1^* improves, it releases more pollutants into the liquid. The enhancement in the impurities will intensify the concentration in the liquid. The Walter’s liquid B fluid shows a higher concentration curve than second-grade fluid. Walter’s liquid B fluid will exhibit higher viscosity, which decreases the dispersion, and slower dissolve of pollutants than second-grade fluid.

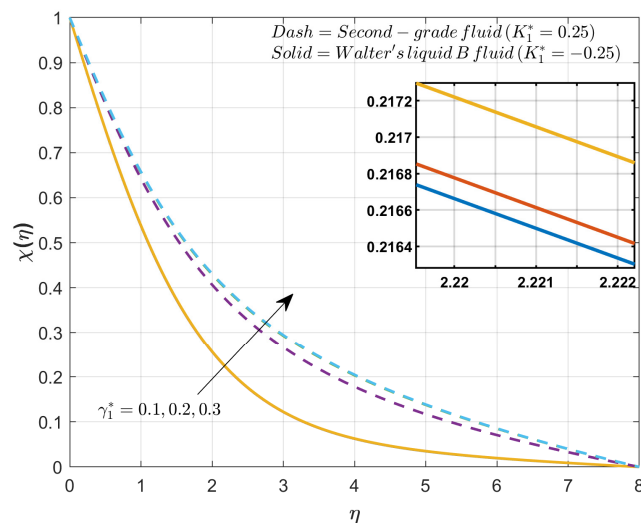


Figure 7. Influence of γ_1^* on χ profile.

Figure 8 shows the impact of ϕ^* on Cf over various values of λ_1^* . The improvement in these two factors will decline Cf . The results show that Walter’s liquid B fluid exhibits

less surface drag force than second-grade fluid in the presence of these two parameters. As λ_1^* improves it will offer additional resistance to the liquid flow and acts as a barrier; the addition of ϕ^* will enhance the thickness of the boundary layer. Due to its higher viscosity and higher tendency for the aggregation of particles, Walter’s liquid B fluid will experience lower C_f than second-grade fluid.

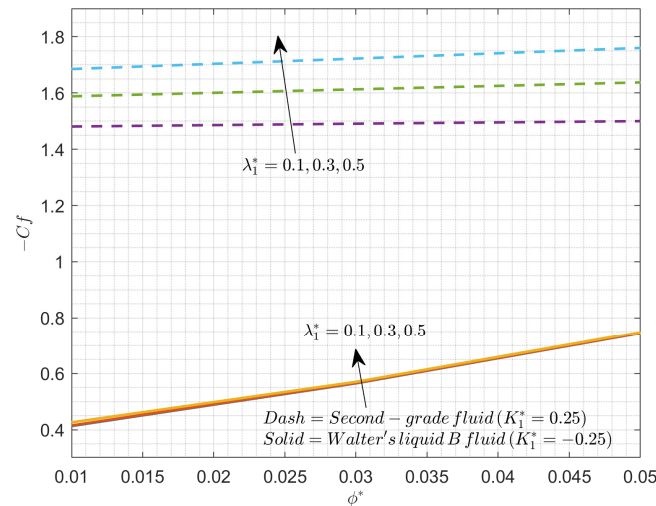


Figure 8. Influence of ϕ^* on C_f for escalated values of λ_1^* .

The influence of ϕ^* on Nu over various values of Rd_1^* is shown in Figure 9. The rise in the values of ϕ^* and Rd_1^* will enhance the thermal distribution rate. The Figure 9 shows second-grade fluid will exhibit a higher rate of thermal distribution than Walter’s liquid B fluid. Rd_1^* exchanges energy among the outermost layer and the surroundings via electromagnetic waves. As a result, an increase in Rd_1^* improves this heat exchange process, resulting in a faster rate of heat transmission. Furthermore, as ϕ^* grows, additional impediments and disruptions in the fluid flow are introduced. This improved contact between liquid and solid particles improves convective heat transfer, resulting in a faster rate of heat transfer at the surface.

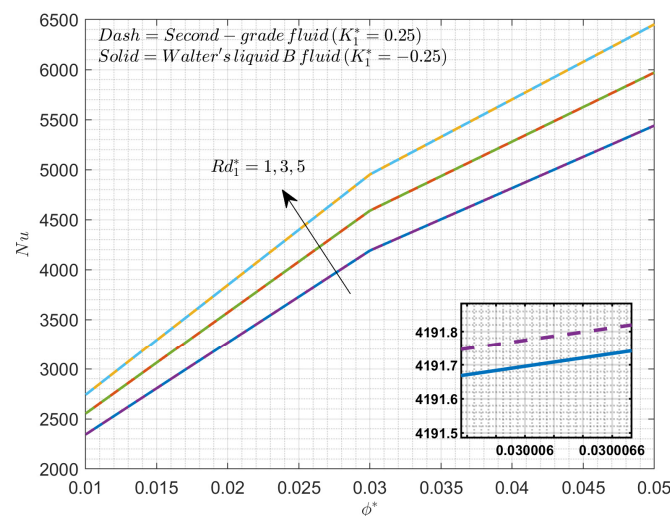


Figure 9. Influence of ϕ^* on Nu for escalated values of Rd_1^* .

Figure 10 display the impact of ϕ^* on Sh over various values of δ_1^* . The improvement in the values of ϕ^* and δ_1^* will decline the rate of mass transfer. Surface mass transfer is affected by alterations in external pollution sources. Higher values of δ_1^* result in increasing surface-level pollution or more rapid change. Pollutant concentration distributions within the liquid

become more pronounced, which slows down the mass transfer rate. More impediments and disruptions are introduced into the fluid flow as the solid volume percentage rises. Because of the increased contact between liquid and solid particles, the surface transfer of mass to contaminants is slowed down. Further from the diagram, it is clear that second-grade fluid will exhibit a lower rate of mass distribution than Walter’s liquid B fluid. Figure 11 shows the streamline pattern for second-grade fluid and Walter’s liquid B fluid in the presence and absence of λ_1^* .

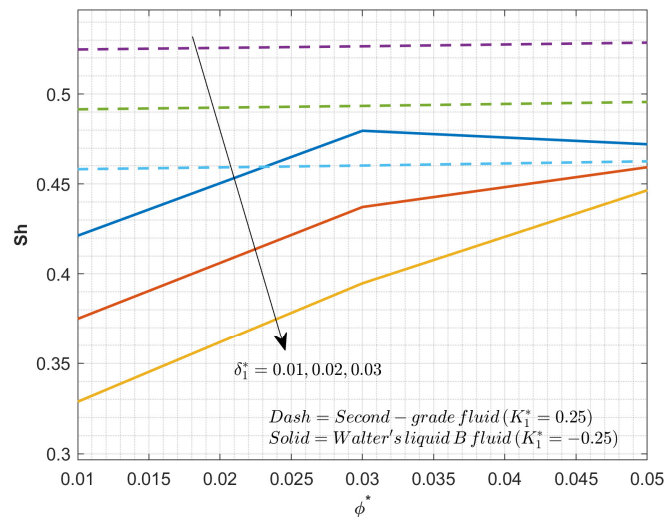


Figure 10. Influence of ϕ^* on Sh for escalated values of δ_1^* .

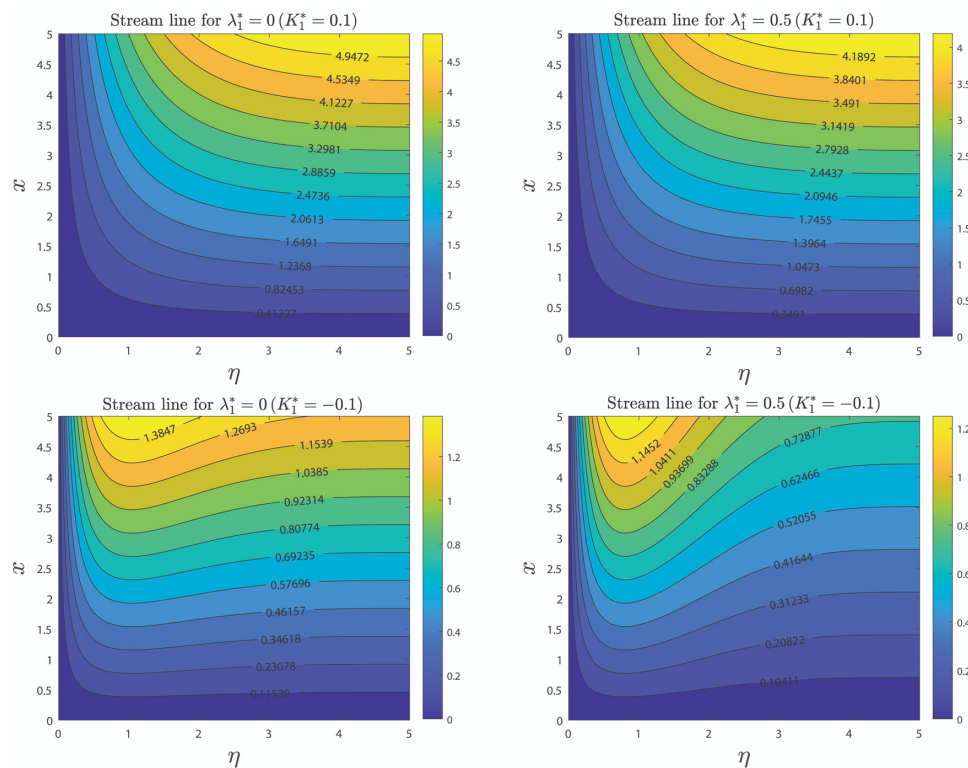


Figure 11. Streamline pattern for second-grade fluid and Walter’s liquid B fluid in the presence and absence of λ_1^* .

Table 5 shows the percentagewise changes in the rate of mass transfer in both second-grade fluid and Walter’s liquid B fluid with respect to changes in the values of δ_1^* and γ_1^* . With the rise in the values of δ_1^* from 0.01 to 0.03, the rate of mass distribution in the

second-grade fluid case will rise from 0.140264% to 0.161919%, while in Walter's liquid B fluid it improves from 0.560122% to 0.601998%. In a similar manner, with improved values of γ_1^* , the rate of mass transfer percentage will decrease from 0.140853% to 0.123269% while in the Walter's liquid B fluid case it is 0.650966% to 0.648976%. Comparing these two liquids, the rate of mass transfer percentage is more in the presence of the nanoparticle than in its absence, and Walter's liquid B fluid shows a greater percentage of rate of mass transfer for these two constraints.

Table 5. Comparison table of rate of mass transfer percentage for second-grade fluid and Walter's liquid B fluid in the presence of δ_1^* and γ_1^* .

Parameter	Values	Second-Grade Fluid	Walter's Liquid B Fluid
		$\left \frac{Sh_{\phi^*=0.01} - Sh_{\phi^*=0}}{Sh_{\phi^*=0}} \right \times 100$	$\left \frac{Sh_{\phi^*=0.01} - Sh_{\phi^*=0}}{Sh_{\phi^*=0}} \right \times 100$
δ_1^*	0.01	0.140264%	0.560122%
	0.02	0.140338%	0.570178%
	0.03	0.161919%	0.601998%
γ_1^*	0.1	0.140853%	0.650966%
	0.2	0.122659%	0.631004%
	0.3	0.123269%	0.648976%

5. Final Remarks

The analysis and discussion of various dimensionless constraints and their influences on flow and thermal and mass transfer in the present investigation will provide valuable insights to the field of environmental protection and management and various engineering areas. The results focus on important factors like the viscoelastic parameter, porosity parameter, radiation, external pollutant source variation parameters, solid volume fraction, and modified Hartmann numbers on their respective profiles. Furthermore, a comparative analysis is made between the second-grade fluid and Walter's liquid B fluid to exhibit their characteristics in the presence of these factors. The major outcomes reveal that an improved porous factor will decline the velocity in both of the fluid cases, while in the presence of the Hartmann number velocity improves in the second-grade fluid case while the opposite trend is observed in the Walter's liquid B fluid case. Thermal distribution and concentration improve with rises in radiation and external pollutant source variation parameters. The addition of volume fraction and porosity will reduce the surface drag force. In the presence of the radiation factor, the rate of thermal distribution will rise. Local pollutant external source parameter and solid volume fractions will decline the rate of mass transfer. The rate of mass transfer percentage will increase by 0.140264% to 0.161919% for the case of second-grade fluid in the presence of nanoparticles. However, for the case of Walter's liquid B fluid, it is upsurges at around 0.560122% to 0.601998% for the local pollutant external source parameter, but the reverse trend is observed for the external pollutant source variation parameter.

These findings help to improve knowledge of pollution management, temperature transportation, and the transfer of mass optimization, allowing for better decision-making and effective planning to safeguard the environment and sustainable engineering practices. The present work can be extended to examine the different non-Newtonian nanofluids with different geometries and physical aspects.

Author Contributions: Conceptualization, K.V.N., V.K. and J.K.M.; methodology, K.V.N., V.K. and J.K.M.; software, K.V.N., V.K. and J.K.M.; validation, C.K., K.V.N., V.K. and J.K.M.; formal analysis, C.K., K.V.N., V.K., A.M.H. and J.K.M.; investigation, A.M.H., U.K., J.S.C. and I.E.S.; resources, I.E.S.; data curation, U.K., J.S.C. and I.E.S.; writing—original draft preparation, C.K., A.M.H., U.K., J.S.C., I.E.S. and E.-S.M.S.; writing—review and editing, C.K., A.M.H., U.K., J.S.C., I.E.S. and E.-S.M.S.;

visualization, E.-S.M.S.; supervision, E.-S.M.S.; project administration, E.-S.M.S.; funding acquisition, E.-S.M.S. All authors have read and agreed to the published version of the manuscript.

Funding: This work was funded by the Researchers Supporting Project number (RSP2023R33), King Saud University, Riyadh, Saudi Arabia.

Data Availability Statement: Not applicable.

Acknowledgments: The authors are thankful for the support of the Researchers Supporting Project number (RSP2023R33), King Saud University, Riyadh, Saudi Arabia.

Conflicts of Interest: The authors declare no conflict of interest.

Nomenclature

Symbols

x and y	Directions
\bar{u} and \bar{v}	Velocity components
M_0	Magnetization of permanent magnets
T^*	Temperature
j_0	Applied current density in electrodes
C	Concentration
D_f	Diffusivity
C_∞	Ambient concentration
C_w	Surface concentration
U_w	Uniform velocity
K^*	Permeability of the porous medium
K_1^*	Viscoelastic constraint
Q_1^*	Modified Hartmann number
Rd_1^*	Radiation constant
Sc^*	Schmidt number
Re	Local Reynolds number
Cf	Skin friction
Nu	Nusselt number
Sh	Sherwood number
F_m^*	Electromagnetic force
T_∞	Ambient temperature
C_p	Heat capacitance
k	Thermal conductivity
q_r	Radiation heat flux
Q^*	Pollutant external source variation parameter
c	Width of the electrodes
b_3^*	Pollutant external source variation parameter
k^*	Absorption coefficient

Greek Letters

α_1^*	Material constant
σ^*	Stefan–Boltzmann coefficient
β_1^*	Parameter related to width and magnitude of electrode
λ_1^*	Porous constant
δ_1^*	Parameter related to local pollutant external source
γ_1^*	Parameter related to external pollutant source variation
ϕ^*	Solid volume fraction
μ	Dynamic viscosity
ν	Kinematic viscosity
ρ	Density
α	Thermal diffusivity

Subscripts

f	Fluid
nf	Nanofluid

References

1. Asogwa, K.K.; Bilal, S.M.; Animasaun, I.L.; Mebarek-Oudina, F.M. Insight into the significance of ramped wall temperature and ramped surface concentration: The case of Casson fluid flow on an inclined Riga plate with heat absorption and chemical reaction. *Nonlinear Eng.* **2021**, *10*, 213–230. [[CrossRef](#)]
2. Madhukesh, J.; Alhadhrami, A.; Kumar, R.N.; Gowda, R.P.; Prasannakumara, B.; Kumar, R.V. Physical insights into the heat and mass transfer in Casson hybrid nanofluid flow induced by a Riga plate with thermophoretic particle deposition. *Proc. Inst. Mech. Eng. Part E J. Process Mech. Eng.* **2021**, 09544089211039305. [[CrossRef](#)]
3. Xu, Y.-J.; Shah, F.; Khan, M.I.; Kumar, R.N.; Gowda, R.J.P.; Prasannakumara, B.C.; Malik, M.Y.; Khan, S.U. New modeling and analytical solution of fourth grade (non-Newtonian) fluid by a stretchable magnetized Riga device. *Int. J. Mod. Phys. C* **2022**, *33*, 2250013. [[CrossRef](#)]
4. Asogwa, K.K.; Goud, B.S.; Shah, N.A.; Yook, S.-J. Rheology of electromagnetohydrodynamic tangent hyperbolic nanofluid over a stretching Riga surface featuring dufour effect and activation energy. *Sci. Rep.* **2022**, *12*, 14602. [[CrossRef](#)]
5. Alshehri, A.M.; Coban, H.H.; Ahmad, S.; Khan, U.; Alghamdi, W.M. Buoyancy Effect on a Micropolar Fluid Flow Past a Vertical Riga Surface Comprising Water-Based SWCNT–MWCNT Hybrid Nanofluid Subject to Partially Slipped and Thermal Stratification: Cattaneo–Christov Model. *Math. Probl. Eng.* **2021**, 2021, e6618395.
6. Prasad, K.V.; Rajashekhar, C.; Mebarek-Oudina, F.; Animasaun, I.L.; Makinde, O.D.; Vajravelu, K.; Vaidya, H.; Mahendra, D.L. Unsteady Magnetohydrodynamic Convective Flow of a Nanoliquid via a Radially Stretched Riga Area via Optimal Homotopy Analysis Method. *J. Nanofluids* **2022**, *11*, 84–98. [[CrossRef](#)]
7. Mandal, G.; Pal, D. Mixed convective-quadratic radiative $\text{MoS}_2\text{-SiO}_2/\text{H}_2\text{O}$ hybrid nanofluid flow over an exponentially shrinking permeable Riga surface with slip velocity and convective boundary conditions: Entropy and stability analysis. *Numer. Heat Transf. Part A: Appl.* [[CrossRef](#)]
8. Ali, Q.; Riaz, S.; Memon, I.Q.; Chandio, I.A.; Amir, M.; Sarris, I.E.; Abro, K.A. Investigation of magnetized convection for second-grade nanofluids via Prabhakar differentiation. *Nonlinear Eng.* **2023**, *12*, 20220286. [[CrossRef](#)]
9. Gowda, R.J.P.; Kumar, R.N.; Jyothi, A.M.; Prasannakumara, B.C.; Sarris, I.E. Impact of Binary Chemical Reaction and Activation Energy on Heat and Mass Transfer of Marangoni Driven Boundary Layer Flow of a Non-Newtonian Nanofluid. *Processes* **2021**, *9*, 702. [[CrossRef](#)]
10. Xia, W.-F.; Animasaun, I.L.; Wakif, A.; Shah, N.A.; Yook, S.-J. Gear-generalized differential quadrature analysis of oscillatory convective Taylor-Couette flows of second-grade fluids subject to Lorentz and Darcy-Forchheimer quadratic drag forces. *Int. Commun. Heat Mass Transf.* **2021**, *126*, 105395. [[CrossRef](#)]
11. Fetecau, C.; Nazar, A.; Khan, I.; Shah, N.A. First exact solution for a second grade fluid subject to an oscillating shear stress induced by a sphere. *J. Nonlinear Sci.* **2018**, *19*, 186–195.
12. Shah, N.A.; Yook, S.-J.; Tosin, O. Analytic simulation of thermophoretic second grade fluid flow past a vertical surface with variable fluid characteristics and convective heating. *Sci. Rep.* **2022**, *12*, 5445. [[CrossRef](#)]
13. Khan, M.I.; Qayyum, S.; Kadry, S.; Khan, W.A.; Abbas, S.Z. Irreversibility Analysis and Heat Transport in Squeezing Nanoliquid Flow of Non-Newtonian (Second-Grade) Fluid Between Infinite Plates with Activation Energy. *Arab. J. Sci. Eng.* **2020**, *45*, 4939–4947. [[CrossRef](#)]
14. Hayat, T. On magnetohydrodynamic flow of second grade nanofluid over a nonlinear stretching sheet. *J. Magn. Magn. Mater.* **2016**, *408*, 99–106. [[CrossRef](#)]
15. Kumar, R.N.; Prasannakumara, B.C.; Gowda, R.J.P. Impact of Diffusion-Thermo and Thermal-Diffusion on the Flow of Walters-B Fluid over a Sheet Saturated in a Porous Medium Using Local Thermal Non-Equilibrium Condition, STRPM. (n.d.). Available online: https://www.researchgate.net/publication/370042091_Impact_of_diffusion-thermo_and_thermal-diffusion_on_the_flow_of_Walters-B_fluid_over_a_sheet_saturated_in_a_porous_medium_using_local_thermal_non-equilibrium_condition (accessed on 15 April 2023).
16. Wakif, A.; Animasaun, I.L.; Khan, U.; Shah, N.A.; Thumma, T. Dynamics of radiative-reactive Walters-b fluid due to mixed convection conveying gyrotactic microorganisms, tiny particles experience haphazard motion, thermo-migration, and Lorentz force. *Phys. Scr.* **2021**, *96*, 125239.
17. Siddique, I.; Shah, N.A.; Abro, K.A. Thermography of ferromagnetic Walter’s-B fluid through varying thermal stratification. *South Afr. J. Chem. Eng.* **2021**, *36*, 118–126. [[CrossRef](#)]
18. Qaiser, D.; Zheng, Z.; Khan, M.R. Numerical assessment of mixed convection flow of Walters-B nanofluid over a stretching surface with Newtonian heating and mass transfer. *Therm. Sci. Eng. Prog.* **2021**, *22*, 100801. [[CrossRef](#)]
19. Chu, Y.-M.; Khan, N.; Khan, M.I.; Al-Khaled, K.; Abbas, N.; Khan, S.U.; Hashmi, M.S.; Qayyum, S.; Kadry, S. Thermophoresis particle deposition analysis for nonlinear thermally developed flow of Magneto-Walter’s B nanofluid with buoyancy forces. *Alex. Eng. J.* **2021**, *60*, 1851–1860. [[CrossRef](#)]
20. Choi, S.U.S.; Eastman, J.A. Enhancing Thermal Conductivity of Fluids with Nanoparticles. In Proceedings of the 1995 International Mechanical Engineering Congress and Exhibition, San Francisco, CA, USA, 12–17 November 1995.
21. Khan, U.; Mebarek-Oudina, F.; Zaib, A.; Ishak, A.; Bakar, S.A.; Sherif, E.-S.M.; Baleanu, D. An exact solution of a Casson fluid flow induced by dust particles with hybrid nanofluid over a stretching sheet subject to Lorentz forces. *Waves Random Complex Media* **2022**, 1–14. [[CrossRef](#)]

22. Gkountas, A.A.; Benos, L.T.; Sofiadis, G.N.; Sarris, I.E. A printed-circuit heat exchanger consideration by exploiting an Al₂O₃-water nanofluid: Effect of the nanoparticles interfacial layer on heat transfer. *Therm. Sci. Eng. Prog.* **2021**, *22*, 100818. [[CrossRef](#)]
23. Madhukesh, J.; Shankaralingappa, B.; Gireesha, B.; Prasannakumara, B. Evaluation of heat and mass transfer characteristics in a nanofluid flow over an exponentially stretchable sheet with activation energy. *Proc. Inst. Mech. Eng. Part E J. Process Mech. Eng.* **2022**, 09544089221074827. [[CrossRef](#)]
24. Haq, I.; Kumar, R.N.; Gill, R.; Madhukesh, J.K.; Khan, U.; Raizah, Z.; Eldin, S.M.; Boonsatit, N.; Jirawattanapanit, A. Impact of homogeneous and heterogeneous reactions in the presence of hybrid nanofluid flow on various geometries. *Front. Chem.* **2022**, *10*, 1032805. [[CrossRef](#)]
25. Dogonchi, A.S.; Hashemi-Tilehnoee, M.; Waqas, M.; Seyyedi, S.M.; Animasaun, I.L.; Ganji, D.D. The influence of different shapes of nanoparticle on Cu-H₂O nanofluids in a partially heated irregular wavy enclosure. *Phys. A Stat. Mech. Its Appl.* **2020**, *540*, 123034. [[CrossRef](#)]
26. Gireesha, B.J.; Prasannakumara, B.C.; Umeshaiyah, M.; Shashikumar, N.S. Three Dimensional Boundary Layer Flow of MHD Maxwell Nanofluid over a Non-Linearly Stretching Sheet with Nonlinear Thermal Radiation. *J. Appl. Nonlinear Dyn.* **2021**, *10*, 263–277.
27. Ramesh, G.K.; Madhukesh, J.K.; Shah, N.A.; Yook, S.-J. Flow of hybrid CNTs past a rotating sphere subjected to thermal radiation and thermophoretic particle deposition. *Alex. Eng. J.* **2023**, *64*, 969–979.
28. Atashafrooz, M.; Sajjadi, H.; Delouei, A.A. Simulation of combined convective-radiative heat transfer of hybrid nanofluid flow inside an open trapezoidal enclosure considering the magnetic force impacts. *J. Magn. Magn. Mater.* **2023**, *567*, 170354. [[CrossRef](#)]
29. Oke, A.S.; Prasannakumara, B.C.; Mutuku, W.N.; Gowda, R.J.P.; Juma, B.A.; Kumar, R.N.; Bada, O.I. Exploration of the effects of Coriolis force and thermal radiation on water-based hybrid nanofluid flow over an exponentially stretching plate. *Sci. Rep.* **2022**, *12*, 21733.
30. Alzahrani, H.A.H.; Alsaiari, A.; Madhukesh, J.K.; Kumar, R.N.; Prasanna, B.M. Effect of thermal radiation on heat transfer in plane wall jet flow of Casson nanofluid with suction subject to a slip boundary condition. *Waves Random Complex Media* **2022**, 1–18. [[CrossRef](#)]
31. Prasannakumara, B.C.; Shashikumar, N.S. Boundary Layer Flow and Heat Transfer of Nanofluid with Fluid Particle Suspension Over a Nonlinear Stretching Sheet in the Presence of Thermal Radiation. *J. Nanofluids* **2017**, *6*, 487–495. [[CrossRef](#)]
32. Thumma, T.; Ahammad, N.A.; Swain, K.; Animasaun, I.L.; Mishra, S.R. Increasing effects of Coriolis force on the cupric oxide and silver nanoparticles based nanofluid flow when thermal radiation and heat source/sink are significant. *Waves Random Complex Media* **2022**, 1–18. [[CrossRef](#)]
33. Atashafrooz, M.; Sajjadi, H.; Delouei, A.A. Interacting influences of Lorentz force and bleeding on the hydrothermal behaviors of nanofluid flow in a trapezoidal recess with the second law of thermodynamics analysis. *Int. Commun. Heat Mass Transf.* **2020**, *110*, 104411. [[CrossRef](#)]
34. Makinde, O.D.; Moitsheki, R.J.; Tau, B.A. Similarity reductions of equations for river pollution. *Appl. Math. Comput.* **2007**, *188*, 1267–1273. [[CrossRef](#)]
35. Cintolesi, C.; Barbano, F.; Di Sabatino, S. Large-Eddy Simulation Analyses of Heated Urban Canyon Facades. *Energies* **2021**, *14*, 3078. [[CrossRef](#)]
36. Chinyoka, T.; Makinde, O.D. Analysis of Nonlinear Dispersion of a Pollutant Ejected by an External Source into a Channel Flow. *Math. Probl. Eng.* **2010**, *2010*, e827363. [[CrossRef](#)]
37. Southerland, V.A.; Anenberg, S.C.; Harris, M.; Apte, J.; Hystad, P.; van Donkelaar, A.; Martin, R.V.; Beyers, M.; Roy, A. Assessing the Distribution of Air Pollution Health Risks within Cities: A Neighborhood-Scale Analysis Leveraging High-Resolution Data Sets in the Bay Area, California. *Environ. Health Perspect.* **2021**, *129*, 037006. [[CrossRef](#)]
38. Chinyoka, T.; Makinde, O.D. Modelling and Analysis of the Dispersal of a Polymeric Pollutant Injected into a Channel Flow of a Newtonian Liquid. *Diffus. Found. Mater. Appl.* **2023**, *33*, 23–56. [[CrossRef](#)]
39. Brewster, M.Q. *Thermal Radiative Transfer and Properties*; John Wiley & Sons: Hoboken, NJ, USA, 1992.
40. Ishak, A.; Nazar, R.; Pop, I. Mixed Convection on the Stagnation Point Flow Toward a Vertical, Continuously Stretching Sheet. *J. Heat Transf.* **2006**, *129*, 1087–1090. [[CrossRef](#)]
41. Abolbashari, M.H.; Freidoonimehr, N.; Nazari, F.; Rashidi, M.M. Entropy analysis for an unsteady MHD flow past a stretching permeable surface in nano-fluid. *Powder Technol.* **2014**, *267*, 256–267. [[CrossRef](#)]
42. Das, S.; Chakraborty, S.; Jana, R.N.; Makinde, O.D. Entropy analysis of unsteady magneto-nanofluid flow past accelerating stretching sheet with convective boundary condition. *Appl. Math. Mech.* **2015**, *36*, 1593–1610.
43. Alwawi, F.A.; Alkasasbeh, H.T.; Rashad, A.M.; Idris, R. Natural convection flow of Sodium Alginate based Casson nanofluid about a solid sphere in the presence of a magnetic field with constant surface heat flux. *J. Phys. Conf. Ser.* **2019**, *1366*, 012005. [[CrossRef](#)]
44. Khan, A.; Khan, D.; Khan, I.; Ali, F.; Karim, F.U.; Imran, M. MHD Flow of Sodium Alginate-Based Casson Type Nanofluid Passing through a Porous Medium with Newtonian Heating. *Sci. Rep.* **2018**, *8*, 8645.

Disclaimer/Publisher's Note: The statements, opinions and data contained in all publications are solely those of the individual author(s) and contributor(s) and not of MDPI and/or the editor(s). MDPI and/or the editor(s) disclaim responsibility for any injury to people or property resulting from any ideas, methods, instructions or products referred to in the content.